


# Construction of approximate invariants for non-integrable Hamiltonian systems

Yongjun Li <sup>1,\*</sup>, Derong Xu,<sup>1</sup> and Yue Hao<sup>2</sup>

<sup>1</sup>Brookhaven National Laboratory, Upton, New York 11973, USA

<sup>2</sup>Michigan State University, East Lansing, Michigan 48864, USA

We present a method to construct high-order polynomial approximate invariants (AI) for non-integrable Hamiltonian dynamical systems, and apply it to modern ring-based particle accelerators. Taking advantage of a special property of one-turn transformation maps in the form of a square matrix, AIs can be constructed order-by-order iteratively. Evaluating AI with simulation data, we observe that AI's fluctuation is actually a measure of chaos. Through minimizing the fluctuations with control knobs in accelerators, the stable region of long-term motions could be enlarged.

The construction of the invariant phase-space tori of Hamiltonian systems is important in many mathematical physics fields (see ref. [1–6] and references therein). For non-integrable Hamiltonian systems, exact solutions for motion are often impossible. They generally lack sufficient conserved quantities. However, Kolmogorov-Arnold-Moser theory [7] proves that approximate invariants (AI) could still exist in such systems. The theory addresses the stability of motion in near-integrable Hamiltonian systems that can be seen as small perturbations of integrable systems. If the perturbation is small enough, a significant portion of the invariant tori of the integrable system survive, though deformed. These surviving tori act as quasi-invariants or AIs, where the motion remains confined and quasi-periodic, preserving the structure of the integrable case. Even though resonances can disrupt some tori, many tori persist in a “cantorized” form, as long as certain non-resonance conditions are met. The remnants of the AI tori provide a structure that partially resists chaotic diffusion, preserving long-term stability in certain regions of phase space. Such region is also known as “dynamic aperture (DA)” in particle accelerator physics [8]. A sufficient DA is often required for beam manipulation and machine operation. It is important to explicitly obtain the AIs of given lattices and evaluate their fluctuations in designing and optimizing modern accelerator magnetic lattice [1, 2].

The evolution of motion in a periodical Hamiltonian system can be approximately represented with polynomial maps. These maps can be extracted with the truncated power series algorithm [9] to any arbitrary order. For example, consider a 4-dimensional phase space vector, which can represent an on-momentum charged par-

ticle's motion in the transverse plane in an accelerator,

$$Z = [x, p_x, y, p_y, x^2, xp_x, xy, xp_y, p_x^2, p_x y, \dots, p_y^\Omega]^T, \quad (1)$$

here the superscript  $T$  represents the transpose of matrices or vectors,  $\Omega$  is its order. Let the one-turn map of the system be written in a square matrix form  $M$  as

$$Z_{final} = MZ_{initial}. \quad (2)$$

Such map is usually non-symplectic due to the truncation. Following the method in Chao's note [10], an  $\Omega$ -order Taylor series approximate invariant  $W$  can be written as

$$W^{(\Omega)} = V^T Z, \quad (3)$$

with  $V$  is the coefficient vector yet to be found. Since  $W$  is an invariant, for any  $Z$  after one-turn transformation through  $M$ , we have

$$V^T Z = V^T MZ \implies V = M^T V. \quad (4)$$

It means that the coefficient vector  $V$  needs to be  $M^T$ 's eigenvector with its eigenvalue as 1. However, when we apply a direct eigen-analysis on the  $\Omega(\geq 3)$ -order matrix  $M^T$ , it usually fails to yield proper AIs. It is because the coefficients of higher orders in  $M^T$  are significantly greater than the lower orders. More specifically, the incremental step at the  $n^{th}$  order is  $n!$ . Therefore, the highest order terms dominate the eigen-analysis, and the obtained eigen-vectors, usually have non-zero coefficients only in the highest order terms. The numerical experiment with simulation data confirms that such AIs are fake. To overcome this difficulty, we introduce a method to start with the well-known linear Wronskian invariants and then iteratively construct higher order AIs by taking advantage of the special property of the square matrix. In this paper, the NSLS-II storage ring [11] is used as

\* email: yli@bnl.gov

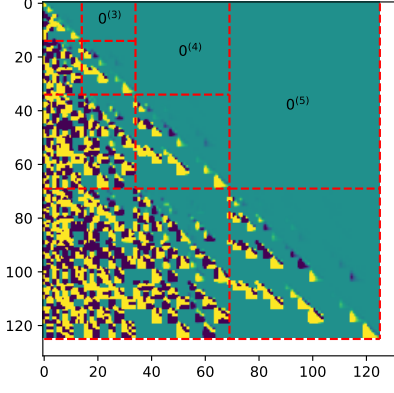


Figure 1. Up to 5<sup>th</sup>-order blocked square matrix  $M^T$ . The first top-left  $14 \times 14$  block is used to construct linear AIs  $W_{1,2}^{(2)}$ . Then the expanded  $34 \times 34$ ,  $69 \times 69$  and  $125 \times 125, \dots$  square matrices are used to obtain high order AIs  $W_{1,2}^{(3,4,5,\dots)}$  respectively, and so on. Note that all elements in the top-right block's ( $0^{(3-5)}$ ) are 0's.

a real-world example for illustration. Its 5<sup>th</sup> one-turn square matrix  $M$  is constructed by sequentially concatenated the magnetic devices as shown in Fig. 1.  $M^T$  matrix is a sparse matrix with its top-right block's elements are always zeros, because any  $n^{\text{th}}$  order term in  $Z$  must be a function of the same and even-higher orders terms ( $\geq n^{\text{th}}$ ), but not of the lower order terms ( $< n^{\text{th}}$ ), i.e.,

$$Z_{final}^n = \sum_{i < n} 0 Z_{initial}^i + \sum_{i \geq n} m_i (\neq 0) Z_{initial}^i \quad (5)$$

This property actually enables us to construct AIs order-by-order iteratively.

We start with the linear invariants, then construct higher order AIs on top of them. Even in the linear case,  $Z$  must be kept up to the quadratic terms in order to find quadratic invariants  $W^{(2)}$ . First, a  $14 \times 14$  square matrix  $M^T$  truncated up to the quadratic terms is used. The eigen-analysis on  $M^T$  yields two eigen-vectors  $V_{1,2}^{(2)}$  with their eigenvalues as 1:

V2_1		V2_2
-----		-----
2 0 0 0		0 0 2 0
4.883952e-02		2.969949e-01
0 2 0 0		0 0 0 2
2.047522e+01		3.367061e+00

Here each monomial is represented with the first four integers as the power indexes of  $x, p_x, y, p_y$ , and the last float as its coefficient. These two invariants can be easily recognized as the normalized Wronskian (aka ‘‘Courant-Synder’’ [12] in accelerator physics) invariants in the

horizontal and vertical planes respectively,  $W_{u=x,y} = \gamma_u u^2 + 2\alpha_u u p_u + \beta_u p_u^2$ , with the Twiss parameters  $\alpha, \beta, \gamma$ . The disappearance of two crossing terms  $x p_x$  and  $y p_y$  terms is simply due to the local  $\alpha_{x,y} = 0$ .

Now we begin to construct cubic AIs by adding some additional terms into linear invariants  $V = [V^{(2)}, V^{(3)}]$ , with  $V^{(3)}$  the cubic coefficients yet to be found. By observing the form of the cubic square matrix  $M^T$  ( $34 \times 34$ ) in Fig. 1, we notice that its upright blocks  $0^{(3)}$  are composed of zeros, therefore, it can be divided into 4 sub-matrices  $M^T = \begin{bmatrix} m_0 & 0^{(3)} \\ m_2 & m_3 \end{bmatrix}$ . Here  $m_0$  ( $14 \times 14$ ) is the

quadratic matrix already analyzed previously,  $0^{(3)}$  ( $14 \times 20$ ) is a zero matrix,  $m_2$  ( $20 \times 14$ ) and  $m_3$  ( $20 \times 20$ ) are two matrices with the cubic term coefficients. The new cubic AIs need to satisfy the following condition:

$$\begin{bmatrix} V^{(2)} \\ V^{(3)} \end{bmatrix} = \begin{bmatrix} m_0 & 0^{(3)} \\ m_2 & m_3 \end{bmatrix} \begin{bmatrix} V^{(2)} \\ V^{(3)} \end{bmatrix}. \quad (6)$$

Because the first row in Eq. (6) is already valid automatically, the cubic term coefficient  $V^{(3)}$  can be simply solved with:

$$V^{(3)} = (I - m_3)^{-1} m_2 V^{(2)}. \quad (7)$$

By solving Eq. (7), the cubic terms in two AIs are obtained as:

V3_1		V3_2
-----		-----
3 0 0 0		1 0 2 0
1.327349e-01		-4.703005e+00
2 1 0 0		1 0 1 1
-6.078392e-01		-1.778960e+00
...		...
0 1 0 2		0 1 0 2
4.370392e+01		-5.597472e+01

The constructed cubic AI's coefficients  $[V^{(2)}, V^{(3)}]^T$  can be compared with its one-turn transformation  $M^T [V^{(2)}, V^{(3)}]^T$  as shown in Fig. 2. The maximum difference of coefficients is below  $1 \times 10^{-13}$ . It is worthwhile to mention that, the existence of the solution in Eq. 7 requires the square matrix  $(I - m_3)$  to be invertible. In some rare cases, this condition might not be satisfied, which means the appearance of broken tori [10]. However, for most stable systems such as accelerators, their  $(I - m_3)$  usually invertible because their fundamental frequency is off-resonant. Once the cubic AIs are obtained, we can iteratively apply Eq. (6) to solve higher order AIs.

Once the AIs are obtained, we can verify them with simulation data. Here a simulated 128 turns trajectory starts with an initial condition  $x = 6.4\text{mm}$ ,  $y =$

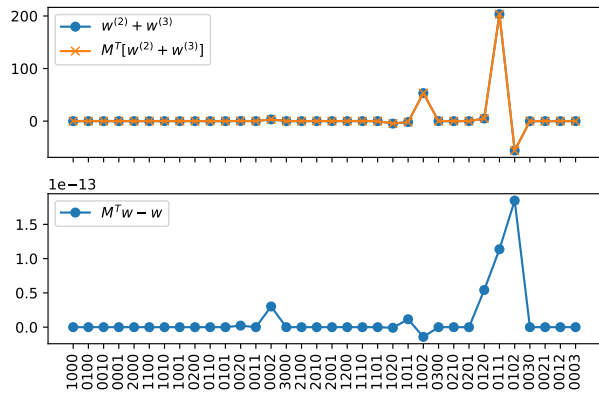


Figure 2. Comparison a 3<sup>rd</sup>-order AI's coefficient  $[V^{(2)} + V^{(3)}]$  with its one-turn transformation  $M^T[V^{(2)} + V^{(3)}]$ . Top: the values of all 34 monomial coefficients. Bottom: the difference between them represents the quality of the AI.

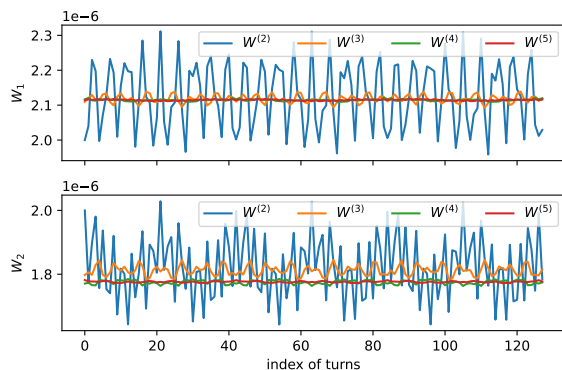


Figure 3. Fluctuations of two AIs  $W_{1,2}^{(2,3,4,5)}$  at different orders ( $2^{nd} - 5^{th}$ ) by evaluating with a simulated trajectory.

2.6mm,  $p_{x,y} = 0$  is obtained with a symplectic tracking algorithm [13]. After substituting the turn-by-turn coordinates into the  $2^{nd}$ - $5^{th}$  AIs  $W_{(1,2)}^{(2,3,4,5)}$ , they are observed converge gradually with reduced fluctuations as illustrated in Fig. 3, which indicates the accuracy of AIs is improved by including more higher order terms. However, AIs' quality becomes worse when their order is above 5 in this specific example. Thus far, it is unclear if the spoiled even-higher-order AIs are due to the accumulated numerical errors, or they simply don't exist at all.

As seen in Fig. 3, these AIs are only approximately constant, rather than exactly. AI's fluctuation after substituting with simulated data is observed to increase gradually with oscillation amplitude as shown in Fig. 4. The fluctuations of linear AIs (aka "the action smear") are traditionally used as a chaos indicator in accelera-

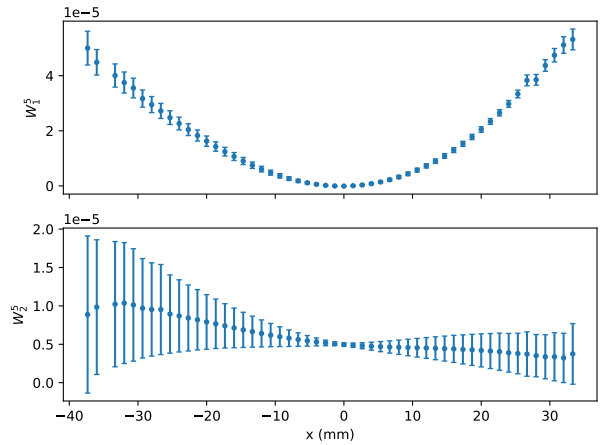


Figure 4. Absolute fluctuations of the 5<sup>th</sup>-order AIs with the horizontal oscillation amplitude (the initial vertical amplitude is 6 mm) in the NSLS-II ring.

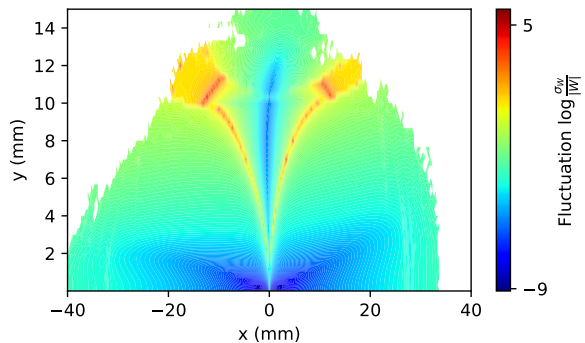


Figure 5. Relative fluctuations of two 5<sup>th</sup>-order AIs within the dynamic aperture in the NSLS-II ring.

tor physics [14]. Once the fluctuations exceed a certain range, approximate tori are broken and the stable particle motion can not be maintained. The relative 5<sup>th</sup>-order AIs' fluctuation defined as  $\frac{\sigma_{W_1}}{|\langle W_1 \rangle|} + \frac{\sigma_{W_2}}{|\langle W_2 \rangle|}$  for the NSLS-II ring is illustrated in Fig. 5. Here  $\sigma_{W_{1,2}}$  represents the standard deviation of multiple-turn  $W$ 's, and  $|\langle W_{1,2} \rangle|$  are their absolute mean values.

In designing accelerators, it is generally believed that, by suppressing the chaos of beam motions, their dynamic apertures can be enlarged. Since the fluctuation of high order AIs are observed to indicate the chaos, we explore the possibility of optimizing the NSLS-II magnetic lattice by suppressing the fluctuations of its 5<sup>th</sup> order AIs. Technically by tuning six family of harmonic sextupoles, we aim to minimize the relative fluctuations of a specific trajectory starting with the initial condition  $x = 15.7\text{mm}$ ,  $y = 3.7\text{mm}$ ,  $p_{x,y} = 0$ . Once the optimal

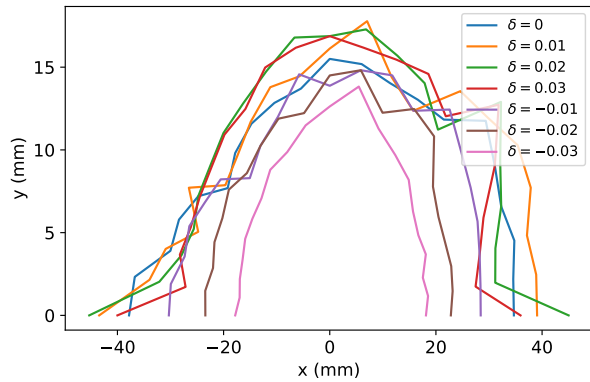


Figure 6. On- and off-momentum dynamic apertures for the optimal solution obtained by minimizing the fluctuations of AIs. Here  $\delta = \frac{\Delta P}{P}$  represents charged particle’s relative momentum deviations.

solution is obtained, its on- and off-momentum dynamic apertures are verified with the tracking simulation code

ELEGANT [15] and illustrated in Fig. 6. The obtained nonlinear lattice performance are similar to our baseline design [11]. However, the optimization through suppressing AI’s fluctuation is more efficient than other multi-particle tracking optimizations, such as [16]. We can accomplish the optimization within several hours even on a single core computer.

In summary, we present a method to construct the approximate invariants of nonintegrable Hamiltonian systems. This method is general for any Hamiltonian systems. And we demonstrate the fluctuation of AIs observed with simulation data is a chaos indicator, which can be used as the objective function for tuning the system to enlarge their stable regions.

We would like to thank Y. Hidaka for providing supports in computation. This research is supported by the U.S. Department of Energy under Contract No. DE-SC0012704 and the DOE HEP award DE-SC0023722.

- 
- [1] J Hagel, *Invariants of betatron motion and dynamic aperture: an analytic approach*, Tech. Rep. LEP-TH/86-22 (CERN, 1986).
- [2] Robert L Warnock, “Close approximations to invariant tori in nonlinear mechanics,” *Physical review letters* **66**, 1803 (1991).
- [3] Mikko Kaasalainen and James Binney, “Construction of invariant tori and integrable hamiltonians,” *Physical review letters* **73**, 2377 (1994).
- [4] Mikko Kaasalainen, “Construction of invariant tori in chaotic regions,” *Physical Review E* **52**, 1193 (1995).
- [5] Alessandra Celletti, Antonio Giorgilli, and Ugo Locatelli, “Improved estimates on the existence of invariant tori for Hamiltonian systems,” *Nonlinearity* **13**, 397 (2000).
- [6] Teemu Laakso and Mikko Kaasalainen, “Canonical methods of constructing invariant tori by phase-space sampling,” *Physica D: Nonlinear Phenomena* **243**, 14–19 (2013).
- [7] Rafael De la Llave *et al.*, “A tutorial on KAM theory,” in *Proceedings of Symposia in Pure Mathematics*, Vol. 69 (Citeseer, 2001) pp. 175–296.
- [8] Alexander Wu Chao, Maury Tigner, Hans Weise, and Frank Zimmermann, *Handbook of accelerator physics and engineering* (World scientific, 2023).
- [9] Martin Berz, “Modern map methods for charged particle optics,” *Nuclear Instruments and Methods in Physics Research Section A: Accelerators, Spectrometers, Detectors and Associated Equipment* **363**, 100–104 (1995).
- [10] Alexander Wu Chao, *Lectures on accelerator physics* (World Scientific, 2020).
- [11] Steve Dierker, “NSLS-II preliminary design report,” Brookhaven National Laboratory (2007).
- [12] Ernest D Courant and Hartland S Snyder, “Theory of the alternating-gradient synchrotron,” *Annals of physics* **3**, 1–48 (1958).
- [13] Haruo Yoshida, “Construction of higher order symplectic integrators,” *Physics letters A* **150**, 262–268 (1990).
- [14] A Chao, D Johnson, S Peggs, J Peterson, C Saltmarsh, L Schachinger, R Meller, R Siemann, R Talman, P Morton, *et al.*, “Experimental investigation of nonlinear dynamics in the fermilab tevatron,” *Physical review letters* **61**, 2752 (1988).
- [15] Michael Borland, *Elegant: A flexible SDDS-compliant code for accelerator simulation*, Tech. Rep. (Argonne National Lab., IL (US), 2000).
- [16] Lingyun Yang, Yongjun Li, Weiming Guo, and Samuel Krinsky, “Multiobjective optimization of dynamic aperture,” *Physical Review Special Topics—Accelerators and Beams* **14**, 054001 (2011).